Available online at www.sciencedirect.com
SCIENCE DIRECT®
Engineering Failure Analysis 11 (2004) 715–725
ENGINEERING FAILURE ANALYSIS
www.elsevier.com/locate/engfailanal

Analysis of low cycle fatigue in AlMgSi aluminium alloys

L.P. Borrego [a,*], L.M. Abreu [b], J.M. Costa [c], J.M. Ferreira [c]

[a] Department of Mechanical Engineering, ISEC, Rua Pedro Nunes, Quinta da Nora, 3030-199 Coimbra, Portugal
[b] Escola Superior de Tecnologia e Gestão de Águeda, 3750 Águeda, Portugal
[c] Department of Mechanical Engineering, University of Coimbra, Polo II, Pinhal de Marrocos, 3030-201 Coimbra, Portugal

Received 10 September 2003; accepted 15 September 2003
Available online 13 February 2004

Abstract

In this study low-cycle fatigue tests were performed in two AlMgSi aluminium alloys with different chemical composition, namely 6082-T6 and 6060-T6 alloys, using standard round specimens and tube specimens, respectively. The tests were undertaken in strain control with a strain ratio $R_\varepsilon = -1$. The cyclic stress–strain curves were determined using one specimen for each imposed strain level. The low-cycle fatigue results are used for the characterisation of the cyclic plastic response and the fatigue live of the alloys. Moreover, the geometry of the hysteresis loops and the occurrence of Masing behaviour are also analysed. The observed behaviour is discussed in terms of the chemical composition of the alloys (Mg_2Si hardening particles and Mn dispersoid content) and fracture mechanisms. Alloy 6060-T6 exhibits nearly ideal Masing behaviour, while alloy 6082-T6 presents significant deviations from the Masing model. The type of cyclic deformation behaviour in AlMgSi alloys seems to be influenced by the dispersoid phase.

Keywords: Fatigue testing; Aluminium alloys; Low-cycle fatigue; Fractography; Fatigue markings

1. Introduction

Age hardened aluminium alloys are of great technological importance. In particular for ground transport systems, when relatively high strength, good corrosion resistance and high toughness are required in conjunction with good formability and weldability, aluminium alloys with Mg and Si as alloying elements (Al–Mg–Si, 6xxx aluminium series alloys) are used.

One of the essential goals in the fatigue process study is the prediction of the fatigue life of a structure or machine component subjected to a given stress–time history. To allow this prediction, complete information about the response and behaviour of the material subjected to cyclic loading is necessary. In addition to the characterisation of the cyclic stress–strain response, quantitative information on resistance to crack initiation and growth are of primary importance.

* Corresponding author. Tel.: +351-239-790700; fax: +351-239-790701.
E-mail address: luis.borrego@dem.uc.pt (L.P. Borrego).

1350-6307/$ - see front matter © 2004 Elsevier Ltd. All rights reserved.
doi:10.1016/j.engfailanal.2003.09.003

Modern life-prediction methods, e.g. based on the *Local Strain Approach*, namely by Neuber's rule [1] or the Molski–Glinka method [2], and Finite Element Analysis applied to fatigue crack initiation [3] or crack propagation [4], assume that an unique relation exists which describes the stress–strain path of cyclic loading during both forward and reverse straining. This behaviour is often termed Masing behaviour [5] and can be considered either a special case or a simplification of the real material behaviour.

The cyclic stress–strain path can be dependent on the material microstructure [6]. Several works have reported that fatigue crack growth in AlMgSi alloys can be highly influenced by the dispersoid content due to Mn or Cr being present [7,8].

The present work intends to analyse the microstructure influence, namely the dispersoid content, on the AlMgSi alloys response to cyclic deformation behaviour. For this purpose low-cycle fatigue tests were performed in two AlMgSi alloys with different chemical composition, one containing Mn and the other with practically no content of this element. In addition the strain-fatigue life relation of the alloys will also be obtained.

2. Experimental

This research was conduced using AlMgSi aluminium alloys with a T6 heat treatment, namely the 6082-T6 and 6060-T6 alloys. The T6 heat treatment corresponds to a conversion of heat-treatable material to the age-hardened condition by solution treatment, quenching and artificial age-hardening. The chemical composition and the mechanical properties are shown in Tables 1 and 2, respectively. It is important to notice that alloy 6060 is practically manganese free.

Low-cycle fatigue tests were performed in a servohydraulic, closed-loop mechanical test machine with 100 kN capacity, interfaced to a computer for machine control and data acquisition. The tests were undertaken, in agreement with ASTM E606 standard [9], using 8 mm diameter round specimens and 3 mm thickness tube specimens for alloy 6082 and 6060, respectively. The round specimens were obtained from extruded round rods with 20 mm diameter, and the tube specimens from thin-walled tubes of 26 and 20 mm of external and internal diameter, respectively. After machining the specimen surfaces were mechanically polished. Fig. 1 illustrates the major dimensions of the samples used in the tests.

Table 1
Main chemical composition of the AlMgSi aluminium alloys (wt%)

Alloy	Si	Mg	Mn	Fe	Cr
6082	1.05	0.80	0.680	0.260	0.010
6060	0.39	0.43	0.007	0.188	0.002

Table 2
Monotonic mechanical properties of the T6 heat treated AlMgSi aluminium alloys

Aluminium alloy	6082	6060
Tensile strength, σ_{UTS} (MPa)	330	240
Yield strength, σ_{YS} (MPa)	307	215
Elongation, ε_r (%)	9	12
Young's modulus, E (GPa)	70	70

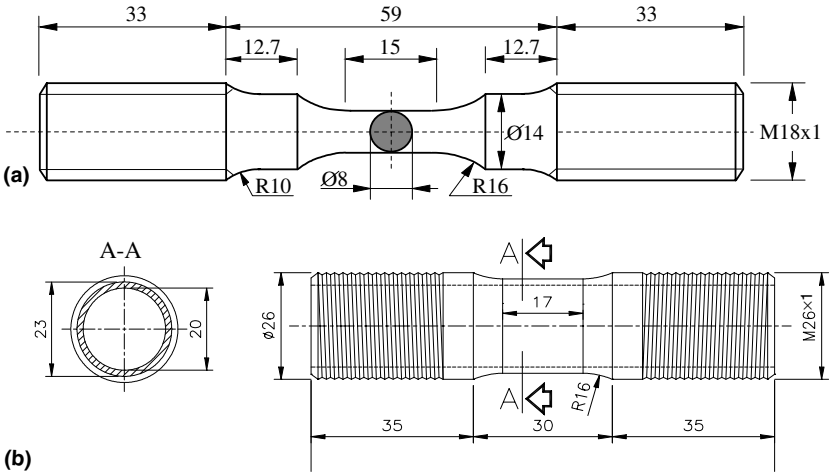

Fig. 1. Geometry of the specimens used in the low-cycle fatigue tests (dimensions in mm): (a) alloy 6082-T6 standard round specimens, (b) alloy 6060-T6 tube specimens.

The samples were cyclically loaded under strain control with symmetrical push-pull loading, i.e., with a nominal strain ratio $R_\varepsilon = -1$. The nominal strain rate $\mathrm{d}\varepsilon/\mathrm{d}t$ was kept constant in all specimens at the value 8×10^{-3} s^{-1} in order to avoid any influence of the strain rate on the hysteresis loop shape. The testing frequency was then calculated as a function of the strain amplitude, $\Delta\varepsilon/2$, by the following equation:

$$f = \frac{\mathrm{d}\varepsilon/\mathrm{d}t}{4(\Delta\varepsilon/2)} \tag{1}$$

The cyclic stress–strain curves were determined using the method of *one specimen for each imposed strain level* and defining the stable hysteresis cycle as the cycle at which the specimens reached 50% of the fatigue life. The specimens were tested with imposed strain ranges between 0.32% and 4%. The failure of each specimen was defined as the number of cycles corresponding to a 30% load drop in relation to the load achieved during the stable hysteresis cycle. The monotonic stress–strain curves were also experimentally determined for comparison. The fracture surfaces were observed in a Philips XL30 scanning electron microscope.

3. Material response to cyclic deformation

The results obtained in the low-cycle fatigue tests are shown in Fig. 2 as the variation of stress amplitude versus the number of strain cycles.

For low strain amplitudes ($\Delta\epsilon/2 < 0.8\%$) the 6082 alloy (Fig. 2(a)) showed cyclic softening, whereas for high strain amplitudes ($\Delta\epsilon/2 > 0.9\%$) cyclic hardening was observed. For intermediate strain amplitudes ($0.8\% \leqslant \Delta\epsilon/2 \leqslant 0.9\%$) the initial hardening stage is followed by long term cyclic softening. In any case, the initial phase of cyclic hardening represented only between 4% and 7% of the fatigue life. The hardening rate (increase rate of the stress amplitude) with strain cycles increased with strain range. Furthermore, the softening rate (decrease rate of the stress amplitude) with strain cycles increases as the strain range decreases. Only a brief initial cyclic hardening stage followed by long term cyclic softening was seen for Alloy 6060 (Fig. 2(b)). The most important changes of cyclic hardening were achieved during the early cycles of

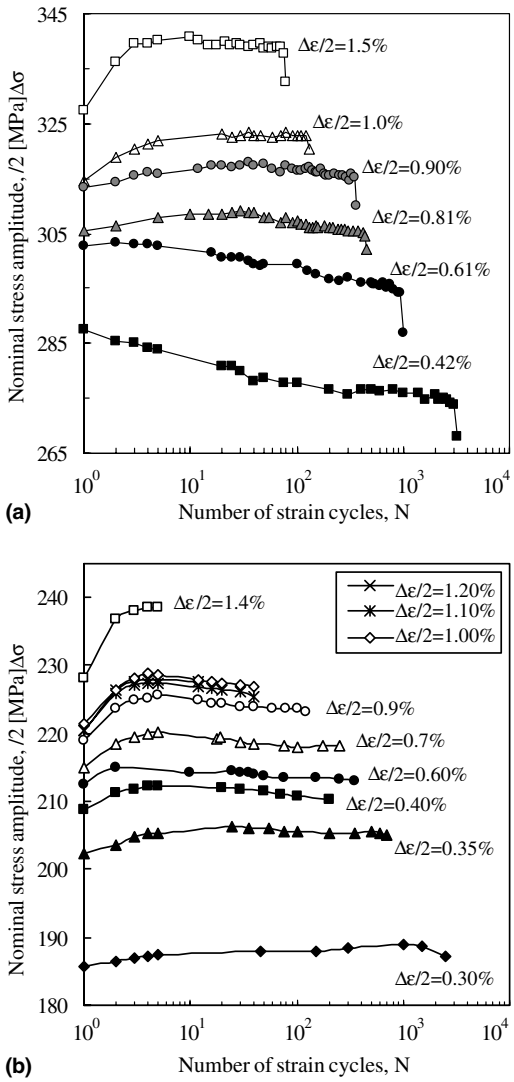

Fig. 2. Variation of stress amplitude for strain cycling: (a) alloy 6082-T6, (b) alloy 6060-T6.

loading, representing approximately to 1% of the fatigue life. Generally, the half life stress amplitude is identical to the stress amplitude of the second strain cycle. For this alloy, an increase of the initial hardening rate with strain cycles was also observed.

The basic stress–strain curve characterises the plastic stress–strain response of the material for the major part of the fatigue life, and is one of its most important fatigue characteristics. The strain hardening exponent and strength coefficient were determined by plotting the stable stress amplitude against the axial plastic strain amplitude on a logarithmic scale. The correlated cyclic stress–strain curves for both alloys are plotted in Fig. 3 and their parameters are indicated in Table 3. The monotonic curves are also superimposed in the figure for comparison.

For alloy 6082, as the cyclic curve lies below the monotonic curve, cyclic softening occurs at low axial strain amplitudes up to 0.82%, while for strain amplitudes higher than 0.82% the alloy cyclically hardens.

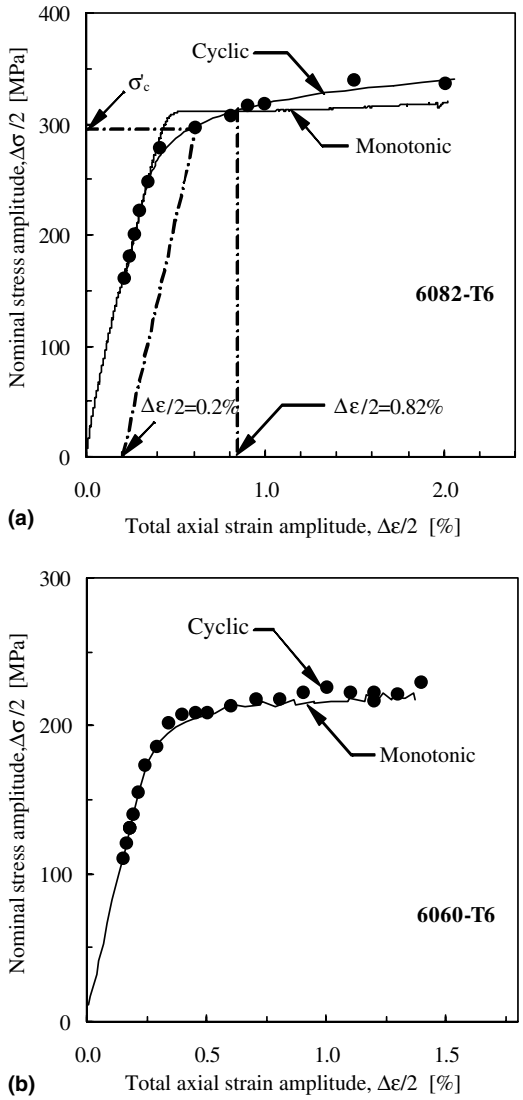

Fig. 3. Monotonic and cyclic stress–strain curves: (a) alloy 6082-T6, (b) alloy 6060-T6.

Table 3
Cyclic stress–plastic strain curve parameters

Aluminium alloy	6082	6060
Cyclic hardening coefficient, k' (MPa)	443.9	267.3
Cyclic hardening exponent, n'	0.064	0.038

The elastic limit for the stress strain curve was reduced from the monotonic value of 307 MPa to the cyclic one of 298 MPa. As expected, alloy 6060 presents a stable cyclic behaviour for approximately all the imposed strain amplitudes analysed. Furthermore, for this alloy, the cyclic yield strength is equal to the monotonic value.

4. Hysteresis loops analysis

Cyclic stress–strain curves are usually expressed by a Ramberg–Osgood stress–strain relationship:

$$\frac{\Delta\sigma}{2} = \frac{\Delta\sigma}{2E} + \left(\frac{\Delta\sigma}{2k'}\right)^{1/n'}, \tag{2}$$

where $\Delta\sigma$ is the stress range, E the Young Modulus, k' the cyclic hardening coefficient and n' the cyclic hardening exponent.

Although Eq. (2) represents the relationship between stress and strain stable amplitudes, it cannot, generally, describe the hysteresis loop branches. A material is said to exhibit Masing [5] behaviour when the magnification of the cyclic stress–strain curve equation by a factor of two describes the branches of the hysteresis loops as schematically shown in Fig. 4. The origin of this curve is at the compressive tip of the corresponding loop. Furthermore, in Masing's model, the stress–strain path after stress reversals follows a unique curve regardless of the amplitude of loading.

Fig. 5 presents the stable stress–strain hysteresis loops, measured at different values of strain amplitude, plotted in relative coordinates corresponding to a translation of the loops ascending branches in such a way that their tips coincide at the positions of the load reversal in compression. Masing behaviour is fulfilled when the branches form a common curve [5].

Fig. 5(b) shows that the ascending branches of the loops obtained for alloy 6060 are almost coincident, exhibiting nearly ideal Masing behaviour. On the contrary, alloy 6082 clearly deviates from the Masing-type behaviour (Fig. 5(a)). However, the magnification of the cyclic stress–strain curve is practically coincident with the ascending branches of the loops obtained for strain ranges up to 1.5%. Therefore, a precise mathematical description of the hysteresis loops for this alloy can still be expected for strain ranges lower than 1.5%.

5. Strain-fatigue life relationship

Fig. 6(a) and (b) present, as a log-log plot, the total strain amplitude versus life in reversals ($2N$) for alloys 6082 and 6060, respectively. In addition to the total strain amplitude, the half-life values of elastic and plastic strain amplitudes are also recorded. The total strain amplitude versus fatigue life for alloy 6082-T6 is also superimposed in Fig. 6(b) for comparison.

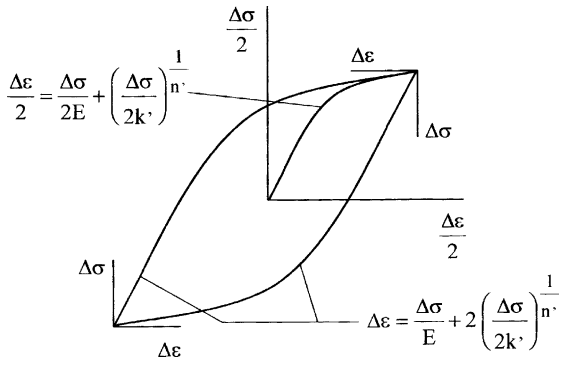

Fig. 4. Masing type material behaviour.

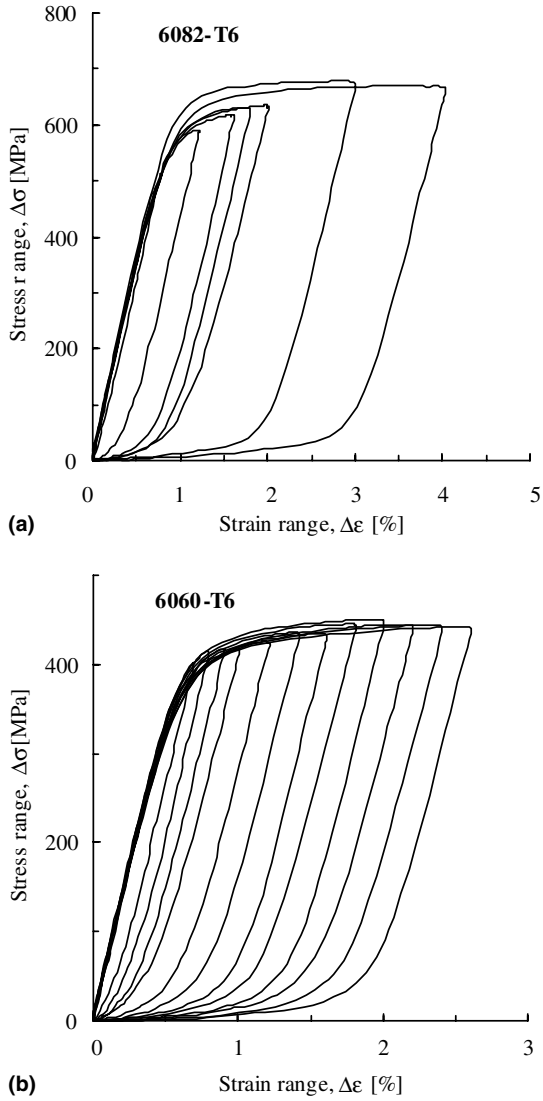

Fig. 5. Superimposed stress–strain loops with matched lower tips: (a) alloy 6082-T6, (b) alloy 6060-T6.

As expected, due to the lower monotonic properties when compared to alloy 6082, alloy 6060 has higher fatigue properties for very high strain amplitudes ($2N \leqslant 100$), but lower fatigue resistance for strain amplitudes less than approximately 2%. The transition life can be determined from these figures. It is defined as the life where the total strain amplitude consists of equal elastic and plastic components, i.e., the life at which the elastic and plastic curves intersect. The transition life was found to be about 744 and 1030 cycles for alloys 6082-T6 and 6060-T6, respectively. Therefore, for higher lives the fatigue resistance of these alloys will be determined by their strength.

The fatigue ductility and strength properties of the alloys were obtained from Fig. 6 and are given in Table 4. Therefore, the strain-fatigue life of the analysed alloys, taking into account the mean stress (σ_m) effect by application of Morrow's equation is for alloys 6082-T6 and 6060-T6, respectively:

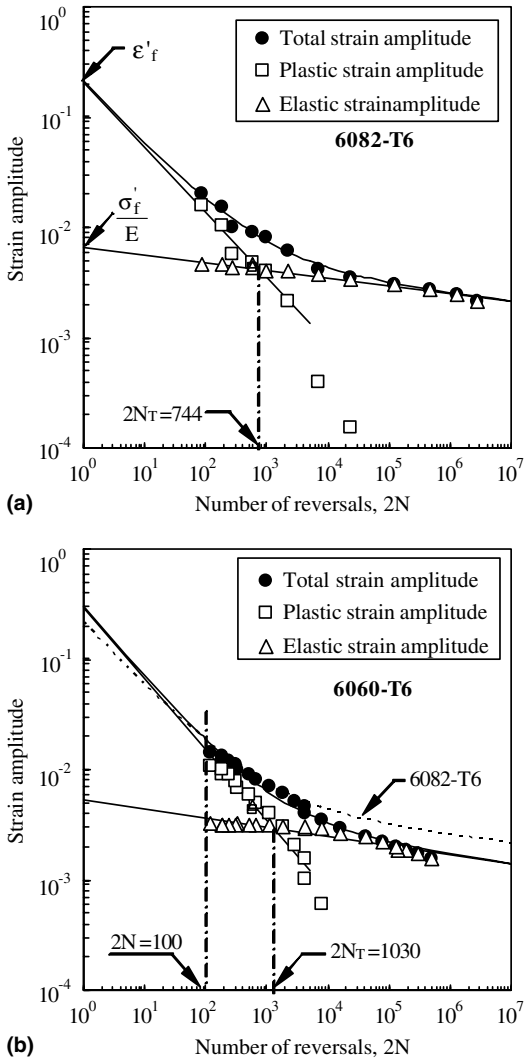

Fig. 6. Life as a function of elastic, plastic and total strain amplitudes: (a) alloy 6082-T6, (b) alloy 6060-T6.

Table 4
Strength and ductility fatigue parameters

Aluminium alloy	6082	6060
Fatigue strength exponent, b	−0.07	−0.084
Fatigue strength coefficient, σ'_f (MPa)	486.8	376.5
Fatigue ductility exponent, c	−0.593	−0.537
Fatigue ductility coefficient, ε'_f	0.209	0.157

$$\frac{\Delta\varepsilon}{2} = \frac{487 - \sigma_m}{70,000}(2N)^{-0.07} + 0.209(2N)^{-0.593}, \tag{3}$$

$$\frac{\Delta\varepsilon}{2} = \frac{377 - \sigma_m}{70,000}(2N)^{-0.08} + 0.157(2N)^{-0.537}. \quad (4)$$

6. Analysis of fatigue fracture surfaces

Fig. 7 shows the typical features of the fatigue fracture surfaces. Fig. 7(a) is a SEM image of the fatigue fracture surface of an 6082-T6 alloy specimen tested at $\Delta\epsilon/2 = 1\%$, while Fig. 7(b) is a SEM image of a 6060-T6 alloy specimen tested at the same imposed strain amplitude. Fig. 7(c) and (d) are high magnification images of Fig. 7(a) and (b), respectively. The images presented were obtained close to the centre of the specimens.

Typical fatigue fracture surfaces of alloy 6082 have a chaotic wavy appearance. Fatigue fractures exhibited relatively smooth areas (labelled A) containing distinct periodic markings (labelled B) generally referred as *tire tracks* because they often resemble the tracks left by a tire. These rows of parallel markings are the result of a particle (or set of particles) on one fatigue fracture surface being successively impressed into the surface of the mating half of the fracture during the closing portion of the fatigue cycle. Fig. 7(c) also shows the occurrence of cleaved particles in voids (labelled C) and widely dispersed microvoid formation around second-phase particles (labelled D). On the other hand, the fatigue fracture surfaces of alloy 6060 are more homogeneous with no distinct features, consistent with the smaller amount of main pre-

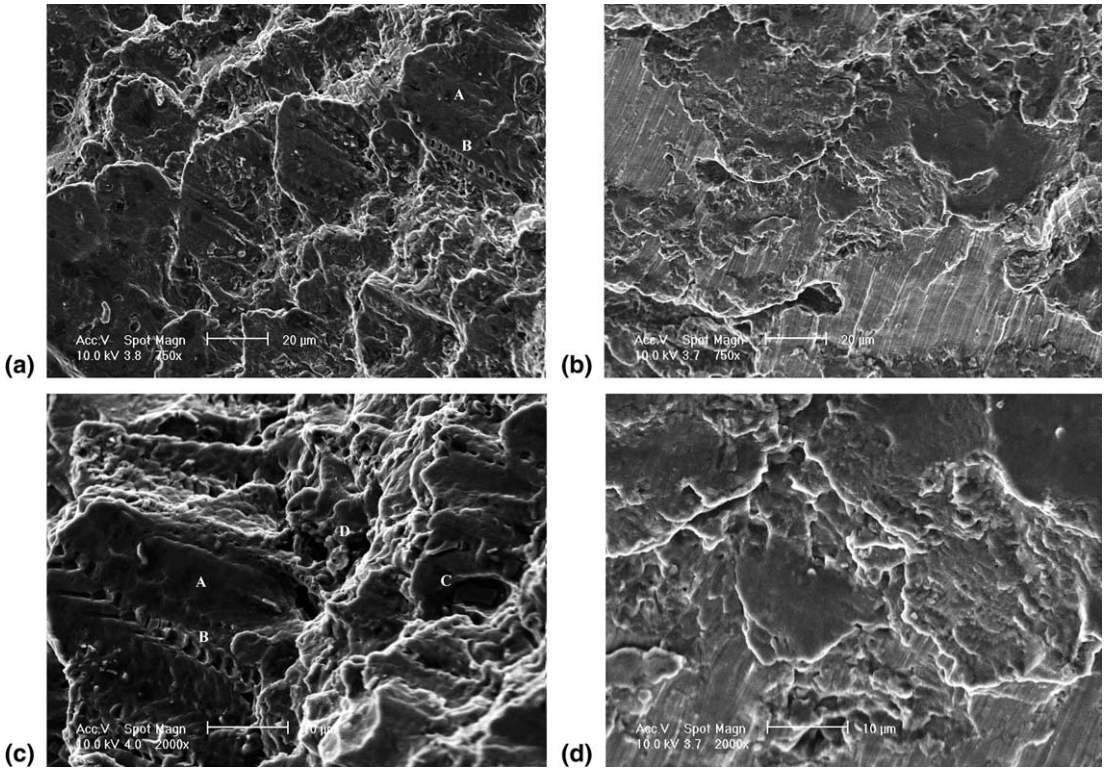

Fig. 7. SEM images of fatigue fracture surfaces, $\Delta\varepsilon/2 = 1\%$. Alloy 6082-T6: (a) and (c), Alloy 6060-T6: (b) and (d).

cipitates (precipitation and solid solution Mg_2Si hardening particles) and the complete absence of the dispersoid phase.

Christ and Mughrabi [6] have shown that an important requirement for Masing-type behaviour in multiple-phase materials is that the particle/dislocation interaction is of minor importance for plastic deformation compared to dislocation interactions. Obviously, the microstructure and the dislocation arrangement are strongly affected by the precipitates. As a result of the dominating effect of the precipitates, which act as strong obstacles to dislocation motion, the dislocation/dislocation interactions are less important and three-dimensional dislocation structures, which are typical of wavy-slip materials, cannot be formed. Although some influence of the Si and Mg contents cannot be discounted, the deviation from the Masing-type behaviour observed for alloy 6082-T6 is mainly attributed to the higher dispersoid content in this alloy. The dispersoid phase is composed of spherical and rod shaped particles, rich in Mn and containing other alloying elements such as Si and Cr, dispersed uniformly in the matrix [7]. This phase enhances particle/dislocation interaction and, thus, promotes non-Masing behaviour. For alloy 6060-T6, the dislocations and their mutual interaction gains importance at the expense of the influence of the precipitates, therefore the alloy presents Masing-type behaviour.

7. Conclusions

From the cyclic deformation behaviour of two AlMgSi alloys with different chemical composition, the following concluding remarks can be drawn:

1. Cyclic softening and hardening for axial strain amplitudes respectively lower and higher than 0.82%, were observed for alloy 6082-T6, whereas alloy 6060-T6 presented stable cyclic behaviour.
2. The ductility and strength properties of both alloys were experimentally determined. The transition fatigue life was found to be about 744 and 1030 cycles for alloys 6082-T6 and 6060-T6, respectively.
3. Alloy 6060-T6 exhibits nearly ideal Masing behaviour and alloy 6082-T6 non-Masing behaviour. However, for alloy 6082-T6, the Masing model can still be used for strain ranges up to 1.5%.
4. The type of deformation behaviour in AlMgSi alloys seems to be influenced by the dispersoid phase. This phase enhances particle/dislocation interaction and, thus, promotes non-Masing behaviour.

Acknowledgements

The authors acknowledge POCTI programme, project 1999/EME/32984, for funding the work reported.

References

[1] Neuber H. Theory of stress concentration for shear strained prismatic bodies with arbitrary nonlinear stress–strain law. J Appl Mech 1961;28:544–51.
[2] Molski K, Glinka G. A method of elasticplastic stress and strain calculation at a notch root. Mat Sci Eng 1981;50:93–100.
[3] Pinho da Cruz JM, Costa JM, Borrego LP, Ferreira JM. Fatigue life prediction in AlMgSi1 lap joint weldments. Int Journal of Fatigue 2000;12:601–10.
[4] Antunes FV, Borrego LFP, Costa JD, Ferreira JM. A numerical study of fatigue crack closure induced by plasticity. Fatigue Fract Eng. Mater Struct 2004; in press.
[5] Masing G. Eigenspannungen und verfestigung beim messing. In: Proceedings of the 2nd International Congress of Applied Mechanics. Zürich: Orell Füssliverlag; 1926. p. 332–5.
[6] Christ H-J, Mughrabi H. Cyclic stress-strain response and microstructure under variable amplitude loading. Fatigue Fract Eng Mater Struct 1996;19:335–48.

[7] Lee DH, Park JH, Nam SW. Enhancement of mechanical properties of Al–Mg–Si alloys by means of manganese dispersoids. Mat Sci Tech 1999;15:450–5.
[8] Scheffel R, Detert K. Near threshold crack propagation and crack closure in Al–Mg–Si alloys with varying manganese concentration. In: Proceeding of the 6th European Conference on Fracture. Amsterdam: UK: EMAS; 1986. p. 1511–21.
[9] American Society for Testing and Materials. Standard test method for measurements of fatigue crack growth rates. Annual Book of ASTM Standards 2000: Volume 03.01, ASTM E 647. p. 591–630.